

Piezoelectric fibers based on silk fibroin with excellent output performance

Wenqiang Zhen(甄文强), Jie Chen(陈杰), Suna Fan(范苏娜), and Yaopeng Zhang(张耀鹏)
Citation: Chin. Phys. B, 2024, 33 (**8**): 088701. DOI: 10.1088/1674-1056/ad51f5

What follows is a list of articles you may be interested in

Subtraction of liposome signals in cryo-EM structural determination of protein—liposome complexes

Shouqing Li(李首卿), Ming Li(李明), Yumei Wang(王玉梅), and Xueming Li(李雪明)
Chin. Phys. B, 2024, 33 (**8**): 088702. DOI: 10.1088/1674-1056/ad4cdb

Physics-embedded machine learning search for Sm-doped PMN-PT piezoelectric ceramics with high performance

Rui Xin(辛睿), Yaqi Wang(王亚祺), Ze Fang(房泽), Fengji Zheng(郑凤基), Wen Gao(高雯), Dashi Fu(付大石), Guoqing Shi(史国庆), Jian-Yi Liu(刘建一), and Yongcheng Zhang(张永成)
Chin. Phys. B, 2024, 33 (**8**): 087701. DOI: 10.1088/1674-1056/ad51f3

Structure, ferroelectric, and enhanced fatigue properties of sol-gel-processed new Bi-based perovskite thin films of $Bi(Cu_{1/2}Ti_{1/2})O_3$-$PbTiO_3$

Wei-Bin Song(宋伟宾), Guo-Qiang Xi(席国强), Zhao Pan(潘昭), Jin Liu(刘锦), Xu-Bin Ye(叶旭斌), Zhe-Hong Liu(刘哲宏), Xiao Wang(王潇), Peng-Fei Shan(单鹏飞), Lin-Xing Zhang(张林兴), Nian-Peng Lu(鲁年鹏), Long-Long Fan(樊龙龙), Xiao-Mei Qin(秦晓梅), and You-Wen Long(龙有文)
Chin. Phys. B, 2024, 33 (**5**): 057701. DOI: 10.1088/1674-1056/ad2a71

Impact of annealing temperature on the ferroelectric properties of $W/Hf_{0.5}Zr_{0.5}O_2/W$ capacitor

Dao Wang(王岛), Yan Zhang(张岩), Yongbin Guo(郭永斌), Zhenzhen Shang(尚真真), Fangjian Fu(符方健), and Xubing Lu(陆旭兵)
Chin. Phys. B, 2023, 32 (**9**): 097701. DOI: 10.1088/1674-1056/aca9c6

RAPID COMMUNICATION

Piezoelectric fibers based on silk fibroin with excellent output performance

Wenqiang Zhen(甄文强), Jie Chen(陈杰), Suna Fan(范苏娜)[†], and Yaopeng Zhang(张耀鹏)[‡]

State Key Laboratory for Modification of Chemical Fibers and Polymer Materials, College of Materials Science and Engineering, Donghua University, Shanghai 201620, *China*

(Received 11 April 2024; revised manuscript received 5 May 2024; accepted manuscript online 30 May 2024)

The self-powered tissue engineering scaffold with good biocompatibility is of great significance for stimulating nerve cell growth. In this study, silk fibroin (SF)-based fibers with regulatable structure and piezoelectric performance are fabricated by dry-spinning and post-treatment. The concentration of SF and calcium ion in spinning dope and the post-treatment affect the conformation transition and crystallinity of SF. As a result, the SF fibers exhibit high piezoelectric coefficient d_{33} (3.24 pm/V) and output voltage ($\sim$ 27 V). Furthermore, these piezoelectric fibers promote the growth of PC-12 cells, demonstrating the promising potential for nerve repair and other energy harvester.

Keywords: silk fibroin, piezoelectric fiber, dry-spinning, conformation transition

PACS: 87.85.jf, 77.84.–s, 81.05.Lg, 83.80.Mc **DOI:** 10.1088/1674-1056/ad51f5

1. Introduction

The peripheral nervous system (PNS) is crucial for managing the body's physiological functions and activities. There are more than 3×10^5 cases of PNS damage per year worldwide,[1,2] which seriously affects the functions of other parts of the human body. Therefore, the effective repair of damaged PNS is of great clinical significance and scientific value. Tissue engineering scaffolds based on polylactic acid (PLA), chitosan, and inorganic boron materials have been widely used in the clinical surgery.[3–5] In addition, it has been confirmed that electrical stimulation (ES) can restore the electrical signal around the PNS to induce axon elongation and myelin sheath regeneration, thus promoting tissue regeneration.[6] Compared with the traditional autograft method, the scaffold materials with self-powered function not only avoid self-injury, but also realize continuous *in vivo* electrical stimulation treatment. Piezoelectric material, which can convert mechanical energy into electric energy, has been widely used in self-powered devices. Currently, the piezoelectric materials including piezoelectric crystals, piezoelectric ceramics, and piezoelectric polymers are extensively studied. Among them, piezoelectric crystals and piezoelectric ceramics display excellent piezoelectric properties, however, the lack of flexibility makes them difficult to match with soft nerve tissues. The biocompatibility of piezoelectric polymer should be furtherly evaluated in the long term. In addition, the subsequent removal of piezoelectric non-biodegradable polymers inevitably causes secondary damage to patients.[7–9] Therefore, it is urgent to develop flexible, biocompatible and biodegradable bio-scaffold materials with good piezoelectric performance.

As one of the most promising natural polymers, silk fibroin (SF) not only possesses adjustable water solubility, light weight, ease of processing, adjustable piezoelectricity and excellent biocompatibility, but also provides cell adhesion binding sites.[10] SF piezoelectric materials are sensitive to small changes in the surrounding environment,[11] which is beneficial for inducing the growth and orientation of neural cells.[12] What is more important is that SF exhibits both shear piezoelectric and longitudinal piezoelectric properties.[13,14] The piezoelectricity can be optimized by adjusting the content of β-sheet. Therefore, SF is expected to prepare wearable and implantable bio-piezoelectric devices, such as electronic skin and bio-therapeutic electronics. For example, Kim *et al.*[15] prepared polyvinylidene fluoride (PVDF)/SF composite mats through electrospinning technique and found that the addition of SF maintained the similar piezoelectric voltages of pristine PVDF, but exhibited improved tensile strength and cell proliferation rate. Pillai *et al.*[16] coated electrically conductive carbon nanofiber (CNF) into SF-woven neural scaffolds to enhance neuronal cell activity. The cell attachment, growth and proliferation on this scaffold were significantly enhanced, demonstrating the great potential for inducing peripheral nerve regeneration and recovery. Therefore, we believe that SF is an ideal material to prepare nerve tissue engineering scaffold. However, at present, the effect of piezoelectric performance of SF-based scaffolds on nerve repair was rarely reported due to the weak piezoelectric property of SF. For example, Fukada[17] reported that the piezoelectric coefficient

[†]Corresponding author. E-mail: fsn@dhu.edu.cn
[‡]Corresponding author. E-mail: zyp@dhu.edu.cn

© 2024 Chinese Physical Society and IOP Publishing Ltd

(d_{33}), one of the most important piezoelectric coefficients, was only 1 pm/V in term of silk. The electrical output of a piezoelectric energy harvesting skins based on SF hydrogel was only 1.5 V.[18] In addition, the electrospun pristine SF membrane exhibited an open-circuit maximum output voltage of 4.5 V after methanol post-treatment.[19] Asmita[20] prepared a bendable SF-metal-free perovskite (SF-MFP) composite film with an enhanced piezoelectric response of 4.5 V. Lisa[21] prepared a flexible SF-based piezoelectric nanogenerator through the electrodeposition technique. This SF-based nanogenerator was capable of generating a maximum open-circuit voltage of 1.02 V under bending. Sohn[22] prepared an electrospun SF piezoelectric film with the output voltage of about 7 V after alcohol post-treatment. The above reported performances were lower than those of inorganic and organic piezoelectric materials. Therefore, it is crucial to improve the piezoelectric property of SF.

In this paper, we fabricated SF piezoelectric fiber through dry spinning method, and regulated the condensed structure of SF molecules through post-treatment. The obtained SF fiber displays superior piezoelectric properties, including the output voltage of 27 V and high d_{33} value of 3.27 pm/V. In addition, the slight finger movement can produce obvious output performance. These SF piezoelectric fibers display the potential to promote the growth of the neural cell, indicating the application value in the field of peripheral nerve injury repair in the future.

2. Experimental methods

2.1. Materials

Bombyx mori cocoons were sourced from Zhejiang Province, China, while calcium chloride ($CaCl_2$, 99.9%) was obtained from Alfa Aesar. Formic acid (FA, 98%) and sodium carbonate (Na_2CO_3, 99.9%) were both acquired from Sinopharm Chemical Reagent Co. Ltd.

2.2. Preparation of dry-spun fibers

The *Bombyx mori* cocoons underwent a dual degumming process, involving the use of a 0.005-wt% Na_2CO_3 solution at 100 °C for 30 min each time. Subsequently, they were thoroughly rinsed with distilled water to effectively remove sericin. The dried degummed silk was promptly dissolved in $CaCl_2$–FA solutions with concentrations of 12%, 15%, and 18% (w/v) for a duration of 8 hours at 25 °C, respectively. This process yielded spinning dopes with various SF concentrations (w/v) of 25%, 30%, and 35%, respectively. Consequently, the obtained spinning dopes were named as 25%SF–12%$CaCl_2$, 30%SF–15%$CaCl_2$, and 35%SF–18%$CaCl_2$. Rotational rheometer (Anton Paar, MCR 302) was used to test the rheological properties of the spinning dopes at (25 ± 0.5) °C. The amplitude scanning was performed at a fixed frequency of 10 rad^{-1}, and the shear strain range was ranging from 0.1 s^{-1} to 100 s^{-1}.

The above SF–$CaCl_2$–FA solutions were used to dry-spin fiber at room temperature (25 °C) through a custom-made equipment (Fig. 1(a)). The needle length was 38 mm, the take-up rates of the collector were 2.62 m/min for 25%SF–12%$CaCl_2$ solution, and 1.05 m/min for 30%SF–15%$CaCl_2$ and 35%SF–18%$CaCl_2$ solutions. The obtained as-spun SF fibers were named as a-25%SF–12%$CaCl_2$, a-30%SF–15%$CaCl_2$, and a-35%SF–18%$CaCl_2$, respectively.

2.3. Post-treatment of SF fibers

To improve the mechanical properties and piezoelectric properties, the as-spun SF fibers were manually stretched at a draw ratio of 3 times, then immersed in 90 vol% ethanol aqueous solution for 1 hour. The post-treated SF fibers were named as p-25%SF–12%$CaCl_2$, p-30%SF–15%$CaCl_2$, and p-35%SF–18%$CaCl_2$, respectively.

2.4. Characterization of SF fiber

Morphology characterization: The surface morphology of the fibers was characterized by SU1000 high-resolution field emission scanning electron microscopy (SEM) at a voltage of 5.0 kV.

Structural characterization The secondary structure of each fiber was characterized by Fourier transform infrared spectroscopy (FTIR). The ATR accessory was used in the test. The wavenumber range was 600 cm^{-1}–4000 cm^{-1}. Synchrotron radiation wide-angle x-ray diffraction (SR-WAXD) experiments were performed at Shanghai Synchrotron Radiation Facility hard x-ray microfocus beamline station (BL15U1). The test parameters were as follows: energy storage ring energy: 3.5 GeV, x-ray energy: 16 keV, x-ray wavelength: 0.07746 nm, spot size: 4.0 μm×2.5 μm, detector model: Rayonix SX-165, diameter: 195 mm, the test distance: 155 mm, exposure time: 60 s, the standard sample: cerium oxide. The 1D-WAXD curve was obtained by azimuthally integrating 2D-WAXD diffractograms. The crystallinity (X_c) of the crystal region was calculated by

$$X_c = \frac{I_c}{I_c + I_a} \times 100\%,$$

where I_c and I_a were the intensities of crystallization zone and amorphous zone, respectively.[23]

Piezoelectric coefficient The piezo-force microscopy (PFM) mode of atomic force microscope (AFM) (Bruker's Dimension Fast Scan) was used to characterize oscillation amplitude (A) of SF fibers and the scan size was set to 10 μm×10 μm, and the scan rate was maintained at 1 Hz. The test temperature and humidity were (25 ± 0.5) °C and (40 ± 5) RH%, respectively. Finally, the effective piezoelectric coefficient d_{33} was calculated from the measured A and

the voltage applied to the sample (V_{AC}) according to the following equation:[24]

$$d_{33} = \frac{A}{V_{AC}}.$$

Electrical output of dry-spun fiber: A homemade equipment (Fig. S3 in supporting information) was used to test the piezoelectric output of SF fibers at (25 ± 0.5) °C and (40 ± 5) RH%. The SF fibers were pasted by a conductive copper glue.

Cell proliferation PC-12 cells are a commonly used neuronal cell line and are neuronally responsive to nerve growth factor (NGF) and sensitive to electrical signals. Among them, undifferentiated PC-12 cells are spherical in shape and without protrusion, which is beneficial to observe the growth behavior of PC-12 cells. Therefore, undifferentiated PC-12 cell was used for cell proliferation experiments. Eighty thousand PC-12 cells were inoculated into each well of a well plate, the substrate of which was covered with SF fibers. The cell culture medium (500 μL/well, 79% RPMI-1640, 15% horse serum, 5% bovine serum, and 1% penicillin–streptomycin solution (P/S)) were added to each well and placed in a 37 °C cell culture incubator for incubation. To assess cell viability, the cell counting kit-8 (CCK-8) was employed. Specifically, 500 μL of CCK-8 solution was added to each well and incubated at 37 °C for 2.5 h. Subsequently, 200 μL of the solution from each well was transferred to a 96-well cell counter and measured using a microplate reader at 450 nm.

Cell growth Undifferentiated PC-12 cells (8×10^4/well) were inoculated into the well plate covered with SF fibers. The well plates with cell culture medium (1.5 mL/well, 96% RPMI-1640, 2% horse serum, 1% bovine serum, 1% P/S, and 20 ng/mL NGF) were incubated in a cell culture incubator at 37 °C. Subsequently, the well plates were ultrasonically stimulated for 10 min every day with the ultrasound intensity of 0.6 W/cm^2. The stimulation was performed with ultrasound and sustained for five consecutive days with a distance of 5 mm between the probe and SF fibers. The growth condition of cells on fibers was observed by polarized light microscope on the first, third and fifth day of the growth experiment, respectively.

3. Result and discussion

The piezoelectric fibers were prepared through dry-spinning method (Fig. 1(a)). All of the SF concentrations in the spinning dopes were higher than 20 wt%, since the SF molecules may be entangled and form interlaced network structures within the solution when the spinning dope exceeds 20 wt%.[25] In order to investigate the spinnability of the three SF–$CaCl_2$ solutions, the rheological properties were characterized (Fig. 1(b)). In the initial state, the viscosity of 35%SF–18%$CaCl_2$ spinning dope was the highest. As the shear process proceeded, shear thinning behavior was observed in all of the spinning solutions, which was attributed to the presence of the entangled chain network in the solution.[26] In addition, the 35%SF–18%$CaCl_2$ solution showed the fastest decay of the viscosity. In the initial stage of shear, the shear force destroyed the entanglement between SF molecules, thereby reducing the viscosity of the solution. At this time, SF moved along the shear direction, and molecular chain rearrangement occurred under the influence of shear force,[25] which was beneficial for the following spinning. The viscosity of spinning dope affected the spinning process, including spinnability and spinning parameter, then resulting in different morphology, structure and property of the obtained fibers. If the viscosity was low, the low entanglement degree of SF molecular chain results in the difficulty of dry-spinning. That is, the spinning solution tends to form a droplet at the spinneret rather than the uniform fiber when the spinning speed is low. If the viscosity was high, the degree of entanglement of SF molecular chains increased, leading to large intermolecular force. In order to overcome these forces and promote the movement of SF, the relative slow spinning speed should be used to induce the formation of uniform fiber. Hence, the spinning speed of the 30%SF–15%$CaCl_2$ and 35%SF–18%$CaCl_2$ systems (1.05 m/min) was slower than that of 25%SF–12%$CaCl_2$ system (2.62 m/min). In addition, the high viscosity of spinning solution leaded larger fiber diameter (Fig. 1(c)). The diameters of the as-spun fibers obtained from low to high solution concentrations were 30 μm, 70 μm, 60 μm, respectively.

There were cracks along the fiber axis on the surface of the SF fibers (Fig. 1(c)). This may be attributed to the evaporation of formic acid. During the dry spinning process, the fiber interior became denser under the action of stretching. The evaporation of the formic acid inside of the fiber lead to the formation of cracks on the fiber surface. Note that the surface of the as-spun fibers was smooth apart from the cracks. However, the rough morphology with axial grooves was appeared after post-drawing the as-spun fiber for three times and immersing in 90-vol% ethanol solution. In addition, the diameters of the fibers were reduced after post-treatment (Figs. 1(c) panels (iv)–(vi)).

The secondary structure of SF is usually analyzed in amide I region (1508 cm^{-1}–1720 cm^{-1}) and amide III region (1180 cm^{-1}–1300 cm^{-1}) of FTIR spectra.[27] In amide I region, the characteristic peaks of β-sheet, β-turn, and random coil/helix are located at 1611 cm^{-1}, 1696 cm^{-1}, and 1650 cm^{-1}, respectively. In amide III region, the characteristic peaks of β-sheet and random coil/helix are centered at 1233 cm^{-1} and 1266 cm^{-1}, respectively.[27–29] All of the as-spun SF fibers only displayed two broad peaks at 1640 cm^{-1} and 1539 cm^{-1}, indicating the amorphous structure (Fig. S1 in supporting information). After post-treatment, the characteristic peak at amide I was shifted to 1620 cm^{-1}, and

became sharper (Fig. 2(a)), which suggested that the post-treatment induced the conformation of SF molecule from random coil/helix to β-sheet. Meanwhile, the quantitative analysis of the secondary structure in the fibers was performed according to the reported method.[23] From Table 1, the content of β-sheet structure of p-30%SF–15%$CaCl_2$ was the highest and about 64.0%. This might be attributed to that the higher the SF concentration, the greater entanglement degree among molecular chains, which was negative to the conformational transition. As a result, the SF molecular chains did not have enough space to rearrange to form β-sheet structure. Meanwhile, calcium ions in the spinning dope may chelate with carboxyl groups of SF molecules, leading to the cross-linking between the hydrophilic portion of SF molecular chain. Consequently, more random coil structures were formed. In addition, water molecule was trapped by calcium ions, then formed hydrogen bonds with SF molecular, which served as cross-linking points.[30] Therefore, when the concentration of calcium ions increases, more randomly curled chains are bound by water molecules and thus cannot be converted to β-sheet. This explains why the β-sheet content increases first and then decreases. In addition, the ethanol solution can evidently induce the transformation of SF from random coil to β-sheet.[23]

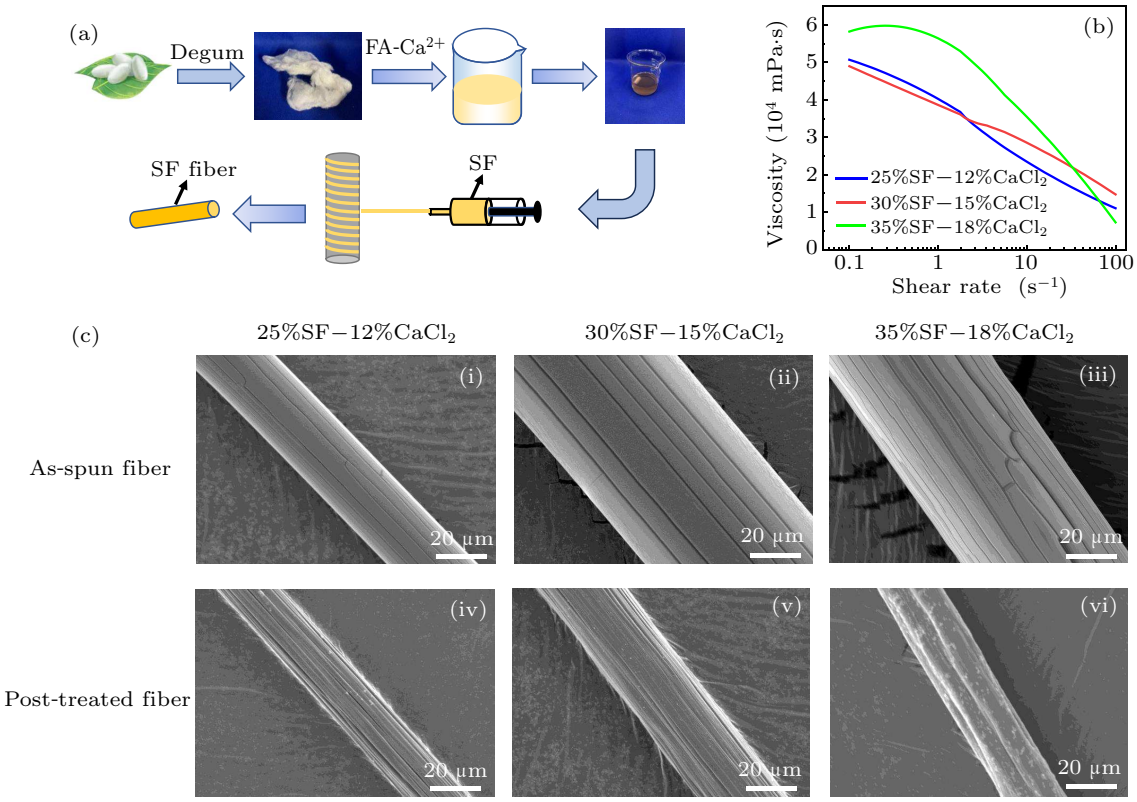


Fig. 1. The preparation of piezoelectric SF fibers. (a) Schematic diagram of the dry-spinning process of SF fibers. (b) Rheological properties of SF solution. (c) SEM images of dry-spun fibers based on different SF–$CaCl_2$ solutions.

Table 1. The content of secondary structure and crystallinity of post-treated SF fibers.

Sample	β-sheet (%)	β-turn (%)	Random coil/helix (%)	Crystallinity (%)
p-25%SF–12%$CaCl_2$	56.9	7.3	35.8	41.70
p-30%SF–15%$CaCl_2$	64.0	11.5	24.5	52.23
p-35%SF–18%$CaCl_2$	61.1	8.5	30.4	48.19

Crystalline structures of SF mainly consist of silk I and silk II. The characteristic diffraction peaks of silk II are mainly located at 9.91°, 10.3°, 12.0°, and 12.7°, which correspond to the lattice planes of (020), (200)/(210), (021), (002), respectively.[31–34] Among them, three lattice planes of (200), (020), (002) represent the direction perpendicular to the molecular chains, the direction perpendicular to the two-dimensional plane, and the direction parallel to the molecular chains, respectively.[34] Compared with the as-spun SF fibers, the post-treated fibers showed the new characteristic diffraction peaks at about 10.3° and 21.4°, which implied the formation of crystalline structure (Fig. 2(b) and Fig. S2 in supporting information). According to the crystallinity calculation method,[23] we obtained that the crystallinities of p-25%SF–12%$CaCl_2$, p-30%SF–15%$CaCl_2$, and p-35%SF–18%$CaCl_2$ were 41.7%, 52.23%, and 48.19%, respectively,

which was consistent with the result of FTIR. As the concentration of calcium ions increases, the number of calcium chelates also increases leading to higher cross-linking between SF molecules. At the meantime, more water molecules were trapped by SF molecular chains to enhance cross-linking reaction. This limited the movement of SF molecules, resulting in lower crystallinity.[30] This is attributed to the structural transformation caused by the synergistic effect of the ethanol molecule and post-stretching. In the post-treated process, ethanol molecules penetrated into the fibers and induced the conformation transition of SF molecular from random coil/helix to β-turn or β-sheet (Fig. 2(c)), the crystal structure is generated. Simultaneously, the tensile force further improved the crystallization. As a result, the crystallinity of SF fibers was enhanced after post-treatment, which were beneficial for the improved piezoelectric performance.

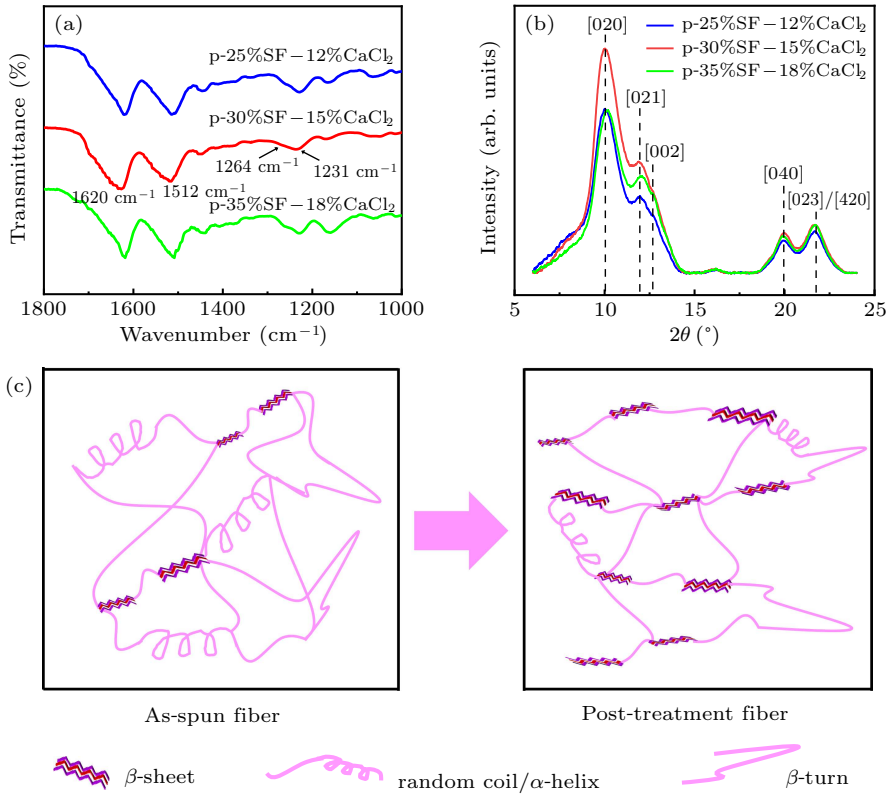


Fig. 2. The structure of dry-spun SF fibers after post-treatment. (a) ATR–FTIR spectra. (b) 1D WAXD diffractograms. (c) The schematics of conformation transformation of SF molecules during the post-treatment process.

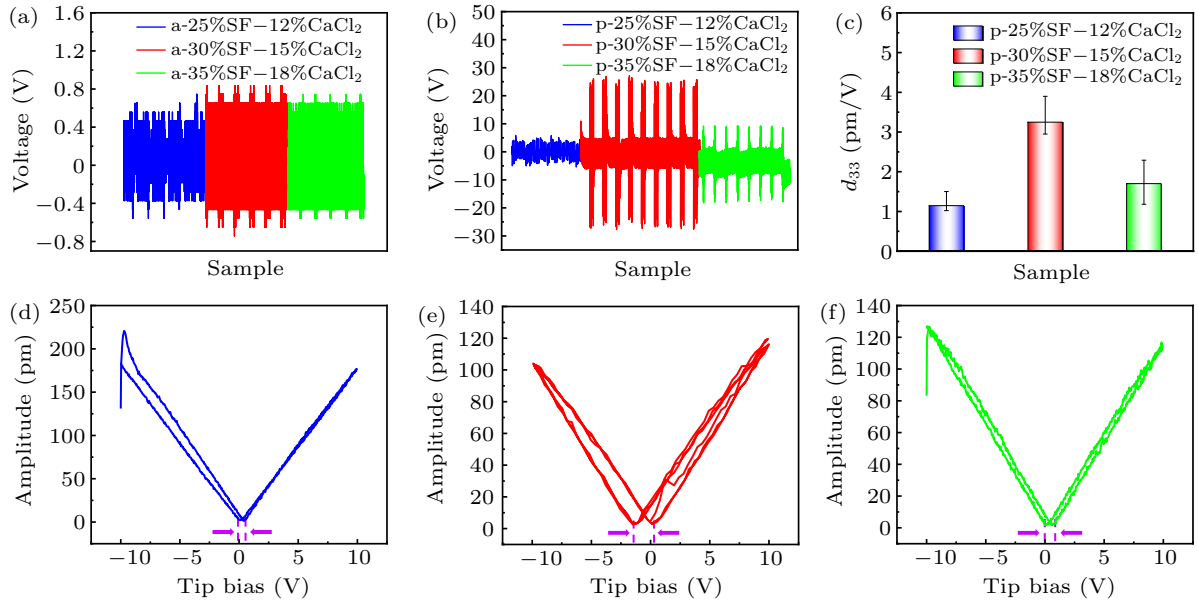


Fig. 3. The piezoelectric performance of different SF fibers. (a)–(b) The output voltage of as-spun (a) and post-treated (b) SF fibers under machine tapping. (c) The d_{33} coefficient of post-treated SF fibers. (d)–(f) Butterfly curves of different SF fibers: p-25%SF–12%$CaCl_2$ (d), p-30%SF–15%$CaCl_2$ (e), and p-35%SF–18%$CaCl_2$ (f).

Moreover, the piezoelectric voltage output of SF fibers was studied. All of the as-spun fibers display output voltage under the external force although the values of the voltage were low (0.6 V–0.9 V) (Fig. 3(a)), demonstrating the intrinsic piezoelectric feature of SF. When a compressive force was applied, the amide dipoles of SF molecules might rotate, resulting in the internal net polarization.[13] After the post-treatment, the output voltage of the p-25%SF–12%$CaCl_2$, p-30%SF–15%$CaCl_2$, and p-35%SF–18%$CaCl_2$ were drastically improved to 6 V, 27 V, and 10 V, respectively. These results suggested that the output voltage of SF fiber increased with the increase of crystallinity. In addition, piezoelectric coefficient d_{33} and butterfly curve were used to characterize piezoelectric performance directly (Figs. 3(d)–3(f)). The d_{33} of p-30%SF–15%$CaCl_2$ fiber was about 3.24 pm/V, which was calculated according to $d_{33} = A/V_{AC}$ (Fig. S4 in supporting information), and three times higher than that of pristine silk (1 pm/V).[17] In addition, this value was larger than those of p-25%SF–12%$CaCl_2$ (1.14 pm/V) and p-35%SF–18%$CaCl_2$ (1.7 pm/V) fibers. The magnitude of d_{33} could also be qualitatively analyzed by the interval between the lowest points of the butterfly curve. Therefore, we could also deduce that the piezoelectric coefficient of p-30%SF–15%$CaCl_2$ system was the largest (Figs. 3(d)–3(f)). These results were consistent with the output voltages (Figs. 3(a) and 3(b)) and solidly confirmed that the crystallization and β-sheet of SF molecular chains were of great significance for the improvement of piezoelectric performance. Based on the performance of the three SF fibers mentioned above, the subsequent study focused on p-30%SF–15%$CaCl_2$ SF fibers.

In order to characterize the output performance of piezoelectric SF fiber, a custom made test equipment was adopted (Fig. S3). The SF fibers were fixed in the middle of two conductive copper layers. Under the external force of 5 N, the output voltage of post-treated fiber was about 5 V, which was higher than that of as-spun fiber (1.5 V) (Figs. 4(a) and 4(b)). With the increase of the amplitude of the external force, the output voltage increased. The highest output voltage reached up to about 20 V under the external force of 25 N (Fig. 4(b)), which outperforms other reported SF-based piezoelectric materials. For example, the output voltage of the electrospun SF composite fibers was only 0.8 V under pressure.[35] The thin SF film doped with ZnO particles output the voltage of 1.7 V at low bending level and 11.2 V at high bending level.[36] In addition, this SF-based piezoelectric device was used to monitor the finger bending deformation (Figs. 4(c) and 4(d)). The output voltages of as-spun and post-treated SF fibers under the slight figure bend were 2 V and 15 V, respectively, suggesting the potential in the application of self-powered tissue scaffold and bio-electronics.

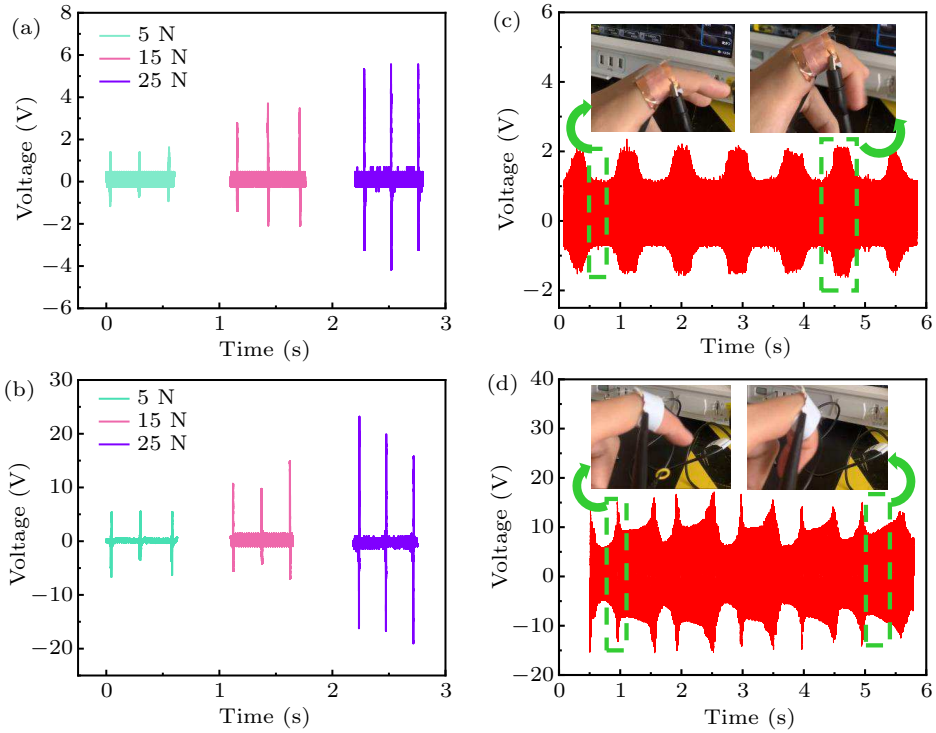


Fig. 4. The piezoelectric performance of [panels (a) and (c)] the as-spun SF fiber and [panels (b) and (d)] the post-treated fiber obtained from 30%SF–15%$CaCl_2$ system. (a)–(b) Output voltage under external forces with different amplitudes.

To verify the effect of piezoelectric performance of SF fibers on the cell proliferation, PC-12 cells were cultured on p-30%SF–15%$CaCl_2$ SF fibers. The result of cell proliferation (Fig. 5(a)) showed that the cell viability gradually increased with time, indicating that the piezoelectric SF fibers displayed good biocompatibility.

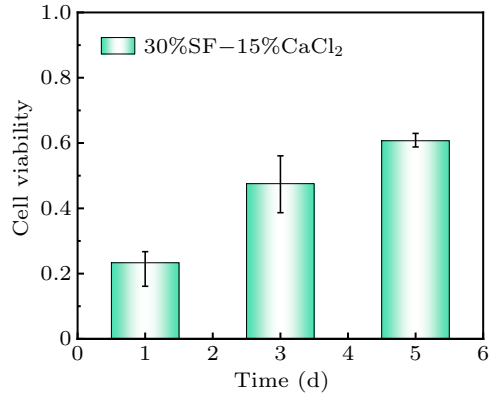


Fig. 5. The proliferation condition of PC-12 cells incubated on the p-30%SF–15%$CaCl_2$ SF fibers for 1, 3, and 5 days.

Meanwhile, to observe the effect of piezoelectric performance of SF fibers on the cell growth, PC-12 cells were cultured on p-30%SF–15%$CaCl_2$ SF fibers under ultrasonic stimulation. Furthermore, the piezoelectric SF fibers had the positive effect on the cell growth especially under the ultrasound stimulation (Fig. 6). After incubating for 1 day, the PC-12 cells tended to adhere on the surface of SF fibers in the shape of a round ball no matter ultrasound stimulation was applied (Figs. 6(a) and 6(d)). When the continuous stimulation lasted for 3 days, the PC-12 cells began to grow to cell protrusions along the axial direction of the fibers (Fig. 6(e)). However, the PC-12 cells still remained a round ball shape without stimulation (Fig. 6(b)). With the ultrasound stimulation was applied for 5 days, the cell protrusions of PC-12 cells continued to grow along the SF fiber axial direction (Fig. 6(f)), while the cell protrusions length of PC-12 cells without ultrasound stimulation hardly increased (Fig. 6(c)). The piezoelectric output of the SF fibers might stimulate the growth of PC-12 cells under ultrasound.[37] Moreover, the SF fibers guided the growth direction of the cell protrusions. The above results suggested that the piezoelectric SF fibers promoted the proliferation and growth of PC-12 cells.

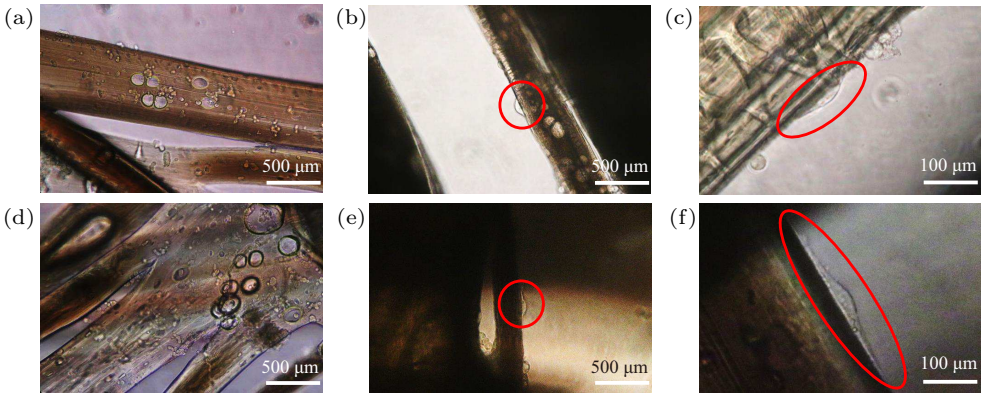


Fig. 6. The growth condition of PC-12 cells incubated on the p-30%SF–15%$CaCl_2$ SF fibers. Without [(a)–(c)] and with [(d)–(f)] ultrasound stimulation for different days. Panels (a) and (d), (b) and (e), and (c) and (f) are 1 day, 3 days, and 5 days, respectively.

4. Conclusions

In summary, we prepared SF fibers with superior piezoelectric performance through dry spinning and confirmed that the high crystalline and β-sheet were beneficial for the improvement of piezoelectric output. The d_{33} and maximal output voltage of the post-treated SF fiber reached up to 3.24 pm/V and 27 V, respectively. In addition, the SF fibers displayed good piezoelectric sensitivity to detect slight finger bending motions. Benefiting from the good biocompatibility and piezoelectric performance, the SF piezoelectric fibers promoted the growth of PC-12 cells under ultrasound stimulation. This indicated the great potential in the application of the future self-powered tissue engineering scaffolds.

Acknowledgements

Project sponsored by the Basic Research Project of the Science and Technology Commission of Shanghai Municipality (Grant No. 21JC1400100), the Shanghai Rising-Star Program (Grant No. 22QA1400400), the National Natural Science Foundation of China (Grant No. 52173031), and the Oriental Talent Plan (Leading Talent Program, No. 152).

References

[1] Zhang J, Zhang B, Zhang J, Lin W and Zhang S 2021 *Front. Cell. Dev. Biol.* **9** 717854
[2] Wang L, Lu C F, Yang S H, Sun P C, Wang Y, Guan Y J, Liu S, Cheng D L, Meng H Y, Wang Q, He J G, Hou H Q, Li H, Lu W, Zhao Y X, Wang J, Zhu Y Q, Li Y X, Luo D, Li T, Chen H, Wang S R, Sheng X, Xiong W, Wang X M, Peng J and Yin L 2020 *Sci. Adv.* **6** eabc6686
[3] Bjelica R, Prpić V, Drvar N, Ćatić A and Gabrić D 2024 *Materials* **17** 1419
[4] Zahedi Tehrani T, Irani S, Ardeshirylajimi A and Seyedjafari E 2024 *Front. Bioeng. Biotech.* **12** 1363241
[5] Jodati H, Evis Z, Tezcaner A, Alshemary A Z and Motameni A 2023 *J. Mech. Behav. Biomed.* **140** 105722
[6] Yao X, Qian Y and Fan C 2021 *J. Mater. Chem. B* **9** 6958
[7] Ali M, Bathaei M J, Istif E, Karimi S N H and Beker L 2023 *Adv. Healthc. Mater.* **12** 2300318
[8] Pina S, Ribeiro V P, Marques C F, Maia F R, Silva T H, Reis R L and Oliveira J M 2019 *Materials* **12** 1824
[9] Orkwis J A, Wolf A K, Mularczyk Z J, Bryan A E, Smith C S, Brown R, Krutko M, McCann A, Collar R M, Esfandiari L and Harris G M 2022 *Biomater. Adv.* **140** 213081

[10] Zou S, Fan S, Oliveira A L, Yao X, Zhang Y and Shao H 2022 *Adv. Fiber Mater.* **4** 758
[11] Wen D L, Pang Y X, Huang P, Wang Y L, Zhang X R, Deng H T and Zhang X S 2022 *Adv. Fiber Mater.* **4** 873
[12] Madduri S, Papaloïzos M and Gander B 2010 *Biomaterials* **31** 2323
[13] Yucel T, Cebe P and Kaplan D L 2011 *Adv. Funct. Mater.* **21** 779
[14] Sencadas V, Garvey C, Mudie S, Kirkensgaard J J K, Gouadec G and Hauser S 2019 *Nano Energy* **66** 104106
[15] Lee J C, Suh I W, Park C H and Kim C S 2021 *J. Tissue Eng. Regen. Med.* **15** 869
[16] Pillai M M, Kumar G S, Houshyar S, Padhye R and Bhattacharyya A 2020 *Nanomed-Nanotechnol* **24** 102131
[17] Fukada E 1956 *J. Phys. Soc. Jpn.* **11** 1301A
[18] Gogurla N, Roy B and Kim S 2020 *Nano Energy* **77** 105242
[19] Sencadas V 2020 *Macromol. Mater. Eng.* **305** 202000165
[20] Veronica A, Liu S, Yang Z, Nyein H Y Y and Hsing I M 2024 *Adv. Mater. Technol.* **9** 2301320
[21] Sarkar L, Yelagala B P, Singh S G and Vanjari S R K 2021 *Int. J. Energ. Res.* **46** 3443
[22] Sohn C, Kim H, Han J, Lee K T, Šutka A and Jeong C K 2022 *Nano Energy* **103** 107844
[23] Zhang C, Zhang Y, Shao H and Hu X 2016 *ACS Appl. Mater. Inter.* **8** 3349
[24] Zhai L, Kim H C, Kim J W and Kim J 2020 *ACS Appl. Bio Mater.* **3** 4329
[25] Hodgkinson T, Chen Y, Bayat A and Yuan X F 2014 *Biomacromolecules* **15** 1288
[26] Um I C, Kweon H, Park Y H and Hudson S 2001 *Int. J. Biol. Macromol.* **29** 91
[27] Ling S, Qi Z, Knight D P, Shao Z and Chen X 2011 *Biomacromolecules* **12** 3344
[28] Chen X, Shao Z, Knight D P and Vollrath F 2007 *Proteins* **68** 223
[29] Chen X, Knight D P and Shao Z 2009 *Soft Matter* **5** 2777
[30] Seo J W, Kim H, Kim K, Choi S Q and Lee H J 2018 *Adv. Funct. Mater.* **28** 1800802
[31] Um I C, Ki C S, Kweon H, Lee K G, Ihm D W and Park Y H 2004 *Int. J. Biol. Macromol.* **34** 107
[32] Drummy L F, Phillips D M, Stone M O, Farmer B L and Naik R R 2005 *Biomacromolecules* **6** 3328
[33] Takahashi Y, Gehoh M and Yuzuriha K 1999 *Int. J. Biol. Macromol.* **24** 127
[34] Shen Y, Johnson M A and Martin D C 1998 *Macromolecules* **31** 8857
[35] Yue X, Wang Z, Shi H, Wu R, Feng Y, Yuan L, Hou S, Song X and Liu L 2023 *Biomater. Sci.* **11** 5232
[36] Sarkar L, Sushma M V, Yalagala B P, Rengan A K, Singh S G and Vanjari S R K 2022 *Nanotechnology* **33** 265403
[37] Chen P, Wu P, Wan X, Wang Q, Xu C, Yang M, Feng J, Hu B and Luo Z 2021 *Nano Energy* **86** 106123